Observation of spatial asymmetry of THz oscillating electron plasma wave in a laser wakefield

Eiji Takahashi,[1,2] Hiroshi Honda,[1] Eisuke Miura,[3] Noboru Yugami,[3] Yasushi Nishida,[3] Keisuke Katsura,[1] and Kiminori Kondo[1]

[1]*Center for Tsukuba Advanced Research Alliance, University of Tsukuba, 1-1-1 Tennodai, Tsukuba, Ibaraki 305-8577, Japan*

[2]*Energy and Environmental Science, Graduate School of Engineering, Utsunomiya University, 7-1-2 Yoto Utsunomiya, Tochigi 321-8585, Japan*

[3]*Electrotechnical Laboratory, 1-1-4 Umezono, Tsukuba, Ibaraki 305-8568, Japan*

(Received 06 January 2000; revised manuscript received 18 April 2000)

The asymmetric spatial distribution of electron density perturbation is observed by using a frequency-domain interferometry technique. The wake amplitude of the outside bump is enhanced by the elliptical distribution of the pump laser pulse. This asymmetry can be explained with a two-dimensional analytical model expanded from cylindrically symmetric linear theory.

PACS number(s): 52.35.Fp, 52.40.Nk, 52.75.Di

With the development of the technology of ultrashort high peak power lasers [1,2], the optical high field is commonly available for experimental research. At the laser intensity of $10^{18}\,\mathrm{W/cm^2}$, the normalized amplitude of the laser field vector potential $a_0 \sim 1$. Here, $a_0 = eA_0/mc^2 = (0.85 \times 10^{-9})\lambda I^{1/2}$ where λ is in μm and I in $\mathrm{W/cm^2}$. Under such a high field, atoms are immediately ionized, and ionized electrons are accelerated by the optical ponderomotive field to a relativistic velocity. If the pulse width of the pumping laser pulse is shorter than the period of the electron plasma oscillation, electrons are expelled from the high field area around the focus of the laser pulse by the ponderomotive force during laser irradiation. After laser irradiation, electron plasma oscillation begins with the frequency of ω_{pe}, where $\omega_{\mathrm{pe}} = (4\pi n_e e^2/m_e)^{1/2}$. Here e, m_e, and n_e are the electron charge, mass, and electron plasma density, respectively. A so-called standard laser wakefield (LWF) [3] starts to oscillate. In the LWF, the longitudinal electric field associated with an electron plasma wave (EPW), of which the phase velocity is almost equal to the speed of light, is thought to be higher than tens of GV/m. This mechanism is very attractive for a compact charged particle accelerator. In experimental research with laser accelerators, several groups have successfully measured accelerated electrons with a self-modulated laser wakefield (SMLWF) [4–6] and a laser beat wave (LBW) [7,8]. Recently, Amiranoff *et al.* [9] also successfully measured accelerated electrons even with the LWF. As is described in Ref. [9], the LWF seems to be the best method for particle acceleration to high energy at present. In both LBW and SMLWF, the EPW is resonantly excited by the laser intensity modulation. In LBW, the resonance condition is more strict than the quasi-resonance in LWF. Although the acceleration physics in a laser accelerator has been confirmed by a number of observations of accelerated electrons, we have many scientific and technical problems in the development of a laser accelerator. To discuss these problems, it is important to get a well-controlled LWF. To control a LWF [10], we have to measure the dynamics of the EPW's. In the measurement of EPW, Hamster *et al.* [11] observed the oscillation of EPW's by measuring THz radiation from the plasma. Marques *et al.* directly measured a temporally and spatially resolved EPW [12,13] by using a frequency-domain interferometry technique [14,15]. In their measurement, the spatial information was obtained from the observation slit of the spectrometer to make a frequency-domain interferometer. Therefore the observation was a one-dimensional (1D) measurement. However, it is necessary to observe two-dimensional (2D) spatially resolved images of EPW's, if we discuss the spatial distortion of the lateral LWF. The lateral LWF is strongly related to the stability of the accelerated electron beam [16] in the LWF accelerator, because it acts as a plasma lens. Thus, it is important for making a LWF accelerator to discuss the effect of the spatial distortion of the lateral LWF.

In this paper, we expanded the frequency-domain interferometry technique in Ref. [12] to two-dimensional measurement. The instantaneous 2D image of the EPW was reconstructed. In this image, we found a cylindrically asymmetric distribution of the relative phase shift caused by the electron density perturbation. This cylindrical asymmetry can be explained with a simple 2D analytical formula modified from cylindrically symmetric theory [17,18].

The frequency-domain interferometry technique in Refs. [10,12,18] was used for observing an EPW in a low density plasma. In our experiment, a 10 Hz Ti:sapphire laser system was used. The pulse width was 100 fs with the maximum output energy as high as 150 mJ per pulse and the spectrum centered at 800 nm. This pulse was separated into two parts by a beam splitter. The reflected part was used as the pump pulse of 60 mJ, and the transmitted part, which was used as the probe pulse, was frequency doubled by a potassium dihydrogen phosphate (KDP) crystal. The probe pulse was sent into a Michelson interferometer, where adequate temporal separation between two colinear pulses was made. The time delay between the two probe pulses and a pump pulse was adjusted by a delay line, which was set after the Michelson interferometer. After mixing the pump and probe pulses at a dichroic mirror, these were focused by a MgF_2 planoconvex lens of $f/4$ in the target chamber. The spot size of the pump pulse at the focal plane was measured to be $7\ \mu\mathrm{m} \times 11\ \mu\mathrm{m}$ [full width at half maximum (FWHM)]. The image of the spot at the focal plane is shown in Fig. 1. The peak intensity was estimated to be $9.9 \times 10^{17}\,\mathrm{W/cm^2}$. The target gas was helium, which filled the target chamber statically. The pres-

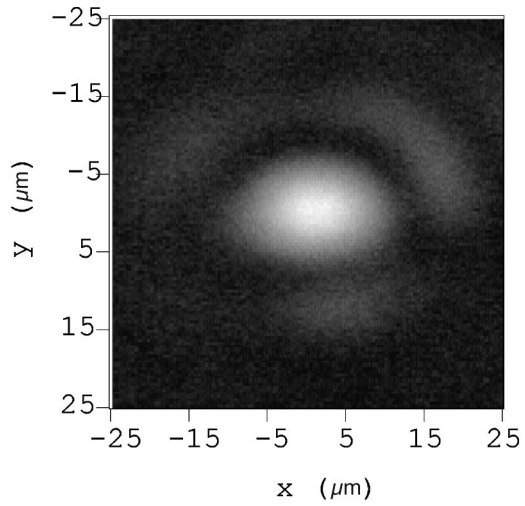

FIG. 1. Typical focal pattern of pump laser pulse at the focal plane.

sure of helium was set to be 0.4 Torr by a capacitance manometer (Baratorn). The pump pulse ionized the helium gas near the focal region and excited an EPW by ponderomotive force. The probe pulses were sent into the area where the EPW was excited. Each pulse causes a phase shift depending on the phase of the EPW, of which the phase velocity is almost equal to the speed of light. These probe pulses were imaged on the spectrometer slit with an $f/2$ doublet, which was set behind the focal point. The pump pulse was reflected before the $f/2$ doublet by an IR mirror. Then only the probe pulses interfered with each other in the spectrometer. The magnification was 31 times. The spectral and spatial resolution of the spectrometer were estimated to be 0.2 Å and 1.2 μm, respectively. The output spectrum was recorded on a 16-bit charge-coupled device camera. The spatially resolved distribution of the relative phase shift can be obtained from the interferogram by Fourier analysis [12,15,18].

When the gas pressure is 0.4 Torr, the electron plasma density n_e is estimated to be $2.6\times10^{16}\,\mathrm{cm}^{-3}$ because of the full ionization of helium. Therefore the period of the electron plasma oscillation T_{pe} is estimated to be 680 fs. In order to obtain the maximum difference of phase shift of the two probe pulses in the interferogram, the time separation of the two probe pulses was adjusted to $1.5T_{\mathrm{pe}}$. First we observed the distribution of the relative phase shift by the plasma, when the pump laser pulse was between the two probe pulses. The phase shift was 100 mrad at maximum. By sweeping the timing of the two probe pulses with a fixed $1.5T_{\mathrm{pe}}$ time interval, the two probe pulses were set to be after the pump pulse. Thus the distribution of the relative phase shift by the EPW was obtained. The typical distribution of the 1D spatial profiles of the relative phase shift is shown in Fig. 2. These profiles in Fig. 2 correspond to the profile along the y axis in Fig. 1. The profile (a) corresponds to the 1D distribution of the relative phase shift at which the first probe pulse is located at the phase of the maximum electron density perturbation and the second at the minimum. The profile (b) shows the phase shift after $0.25T_{\mathrm{pe}}$ from the time of (a). Because the two probe pulses are located at the same phase of the EPW at the time of (b), the relative phase shift became zero. The profile (c) shows the phase shift after

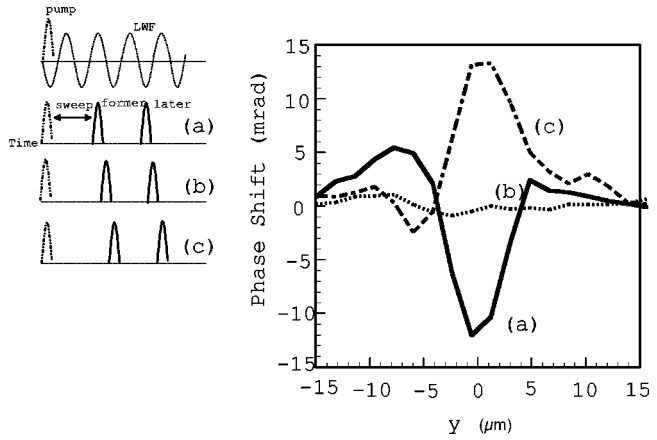

FIG. 2. Spatial distribution of relative phase shift. The profile (a) corresponds to the 1D distribution of the relative phase shift when the first probe pulse is located at the phase of the maximum electron density perturbation and the second at the minimum. The profile (b) shows the phase shift after $0.25T_{\mathrm{pe}}$ from the time of (a). The profile (c) shows the phase shift after $0.5T_{\mathrm{pe}}$ from the time of (a).

$0.5T_{\mathrm{pe}}$ from the time of (a). Since the two probe pulses are located at the reverse phase of the EPW compared to (a), the profile (c) is the reversed profile (a). In profiles (a) and (c), the spatial profile is composed of two parts. One is a central part at $|y|<4$ μm, and the other is an outside part. The central part of the profile can be caused by expulsion of electrons from the laser propagation axis, so that the electron density increases outside the focus. The bump of the phase profile in the outside part is caused by this phenomenon, which will be discussed later.

In 2D imaging, we moved the observation slit of the spectrometer along the x axis in Fig. 1. At each x point, the 1D spatial distributions of the relative phase shift by the EPW were obtained. By placing the 1D distributions obtained in order, we can reconstruct the 2D distribution. In Fig. 3(a), the experimentally obtained instantaneous 2D image of the EPW is shown. 2D electron cavitaion is apparently seen. The solid curves in Fig. 4 show the spatial profiles of electron density perturbation along the lines A-A' and B-B' in Fig. 3(a). Note that the electron density perturbation is normal-

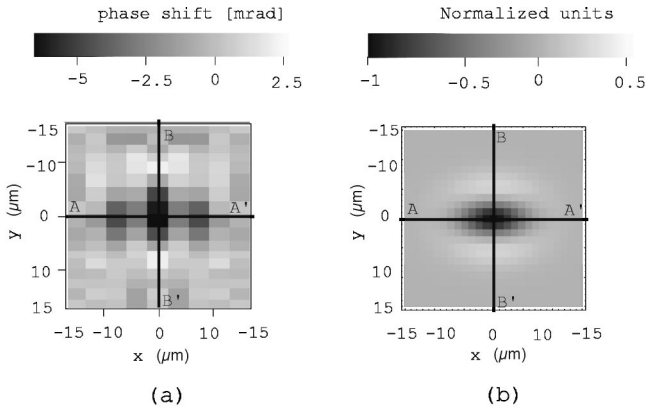

FIG. 3. (a) Experimental 2D spatial distribution of phase shift. (b) 2D spatial distribution of electron density, which is calculated by using the 2D analytical model.

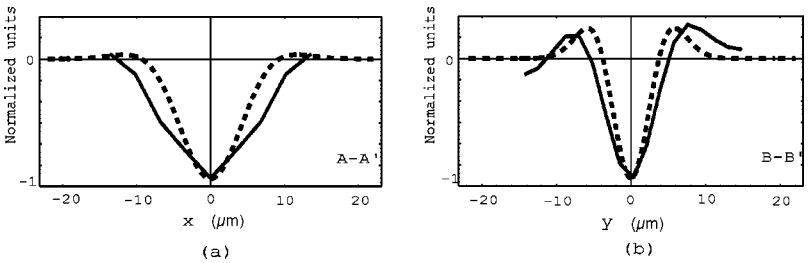

FIG. 4. 1D spatial electron density distribution. Profile (a) corresponds to A-A' in Fig. 4, and profile (b) corresponds to the B-B'. Solid curves: experimental data. Broken curves: numerical fit from the 2D analytical model.

ized in Fig. 4. Cylindrical asymmetry can be also observed. This asymmetry is thought to be caused by the asymmetry of the laser spot at the focal plane, as shown in Fig. 1. As is shown in Fig. 4, the width of the central part of the profile is different between A-A' and B-B'. Moreover, only in the outside part of B-B' can the bump of the phase shift be clearly seen.

In order to analyze this 2D spatial distribution, we derived a theoretical model that describes the cylindrical asymmetry. A two-dimensional cylindrically symmetric formula for the nonrelativistic analytical model has been developed by Gorbunov and Kirsanov and by Marques *et al.* [17,18]. In order to analyze the cylindrically asymmetric distribution of the electron density perturbation, we took the azimuthal angle dependence into account. In the elliptical intensity distribution, the laser intensity at the focal plane can be described by $I(r,\theta,z,t)=I_0\exp[-r^2/s(\theta)^2]\exp[-(t-z/c)^2/\tau_0^2]$, where $s(\theta)$ is defined as $1/\sqrt{(\cos\theta/\sigma_x)^2+(\sin\theta/\sigma_y)^2}$. σ_x and σ_y are the laser focal spot radii along the x and y axes. τ_0 is the laser pulse width. r and θ are the distance from the z axis and the azimuthal angle in cylindrical coordinates, respectively. By defining $\eta=\sigma_x/\sigma_y$ and $\sigma=\sigma_x$, $s(\theta)=\sigma/\kappa(\theta)$ and $\kappa(\theta)=\sqrt{\cos^2\theta+\eta^2\sin^2\theta}$ are obtained. When $\eta=1$, the spot profile becomes a cylindrically symmetric Gaussian distribution. The scalar potential $\phi(r,\theta,z,t)$ can also be described by the following relations from Ref. [18]:

$$\phi(r,\theta,z,t)=\varphi\sin(\omega_{\mathrm{pe}}t-k_{\mathrm{pe}}z)\exp\left[-\frac{r^2}{s^2(\theta)}\right], \qquad (1)$$

where $\varphi=\sqrt{\pi}(I_0/ecn_{\mathrm{c}})(\omega_{\mathrm{pe}}\tau_0/2)\exp[-(\omega_{\mathrm{pe}}\tau_0/2)^2]$. n_{c} is the critical plasma density. The electron density perturbation δn can be obtained from the Poisson law,

$$\delta n=(\epsilon_0/e)\nabla^2\phi=(\epsilon_0/e)\left[\frac{1}{r}\frac{\partial}{\partial r}\left(r\frac{\partial}{\partial r}\right)+\frac{1}{r^2}\frac{\partial^2}{\partial\theta^2}+\frac{\partial^2}{\partial z^2}\right]\phi.$$

Here ϵ_0 is the vacuum permittivity. The electron density perturbation is the sum of two parts, $\delta n=\delta n_{r,\theta}+\delta n_z$. δn_z indicates the longitudinal oscillation of the LWF, which is induced by the temporal profile of the laser pulse, and $\delta n_{r,\theta}$ indicates the transverse oscillation of the LWF, which is induced by the transverse profile of the laser pulse. $\delta n_z/n_{\mathrm{e}}$ and $\delta n_{r,\theta}/n_{\mathrm{e}}$ become

$$\frac{\delta n_z}{n_{\mathrm{e}}}=A\exp\left[-\left(\frac{r}{s(\theta)}\right)^2\right]\sin\left[\omega_{\mathrm{pe}}\left(t-\frac{z}{c}\right)\right] \qquad (2)$$

and

$$\frac{\delta n_{r,\theta}}{n_{\mathrm{e}}}=\left(\frac{2c}{\omega_{\mathrm{pe}}\sigma}\right)^2\left[\frac{\eta^2+1}{2}-\frac{r^2(\eta^2-1)^2}{\sigma^2}\times\cos^2\theta\sin^2\theta-\frac{r^2}{\sigma^2}\kappa^4(\theta)\right]\frac{\delta n_z}{n_{\mathrm{e}}}, \qquad (3)$$

where $A\sim 21P(\mathrm{TW})\times\eta(\lambda/\sigma)^2(\omega_{\mathrm{pe}}\tau_0/2)\exp[-(\omega_{\mathrm{pe}}\tau_0/2)^2]$, P is the instantaneous laser power, and λ is the wavelength of the laser pulse. Therefore, $\delta n/n_{\mathrm{e}}=\delta n_z/n_{\mathrm{e}}+\delta n_{r,\theta}/n_{\mathrm{e}}$. In this measurement, the spot size was measured to be 7 μm$\times$11 μm FWHM. Then σ and η were assumed to be 6.6 μm and 1.57, respectively. Under our experimental conditions, the longitudinal oscillation is negligible compared to the transverse one. Then, $\delta n/n_{\mathrm{e}}$ was approximated as $\delta n/n_{\mathrm{e}}\sim\delta n_{r,\theta}/n_{\mathrm{e}}$. In Fig. 3(b), the theoretically calculated 2D image of $\delta n/n_{\mathrm{e}}$ is shown. To compare the experimentally obtained image with the theoretical one, 1D spatial profiles of A-A' and B-B' are plotted simultaneously in Figs. 4(a) and 4(b), respectively. In these figures, solid and broken curves correspond to the experimental and theoretical data, respectively. The theoretical data are in good agreement with the experiment.

The wake amplitude of the outside bump in the y direction is larger than that in the x direction. As seen in Fig. 4, the ratios R of the normalized wake amplitude $|\delta n/n_{\mathrm{e}}|$ at the outside bump to that at the central part are not fixed to be $1/e^2\sim 0.14$, which can be derived from the cylindrically symmetric theory [18]. According to our model, the ratio $R(\theta,\eta)$ is given by $R(\theta,\eta)=2\psi(\theta,\eta)/(\eta^2+1)\exp[-(\eta^2+1)/2\psi(\theta,\eta)-1]$, where $\psi(\theta,\eta)=(\eta^2-1)^2\cos^2\theta\sin^2\theta/\kappa^2(\theta)+\kappa^2(\theta)$. In the elliptical intensity distribution of the laser pulse, the ratio R depends on θ as shown in Fig. 5. In this figure, the solid curve was estimated by the theory described above for $\eta=1.57$. This ratio for the cylindrically symmetric case is also represented by the dashed line. The two dots in

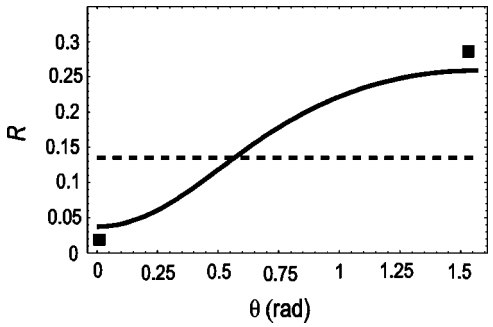

FIG. 5. The ratio R of the normalized wake amplitude $|\delta n/n_{\mathrm{e}}|$ at the outside bump to that at the central part of the profile. Solid line: $\eta=1.57$. Broken line: $\eta=1$. Dots: experimental data.

Fig. 5 were evaluated from the experimental data. For example, the ratio at $\theta=\pi/2$ for $\eta=1.57$ is estimated to be 0.26. This value is about two times larger than that for $\eta=1$. Therefore, the enhancement of the wake amplitude for the outside bump can be attributed to the elliptical intensity distribution.

In conclusion, we observed the spatially distorted electron density perturbation of the lateral LWF. The spatial distribution of the asymmetric electron density perturbation was determined from the elliptical distribution of the pump laser pulse. In the elliptical intensity distribution of a pump laser pulse, the wake amplitude of the outside bump is enhanced along the steeper intensity gradient. A 2D analytical model can explain the experimentally obtained spatial distribution of the asymmetric electron density perturbation.

This work was supported by the Research Foundation for Opto-Science and Technology, University of Tsukuba TARA Project, and a Grant-in-Aid for Scientific Research by the Japanese Ministry of Education, Science, Sport and Culture (Grant No. 11650039).

[1] Y. Nabekawa *et al.*, Opt. Lett. **23**, 1384 (1998).
[2] K. Yamakawa *et al.*, Opt. Lett. **17**, 1131 (1998).
[3] T. Tajima and J. M. Dawson, Phys. Rev. Lett. **43**, 267 (1979).
[4] K. Nakajima *et al.*, Phys. Rev. Lett. **74**, 4428 (1995).
[5] A. Modena *et al.*, Nature (London) **377**, 606 (1995).
[6] C. A. Coverdale *et al.*, Phys. Rev. Lett. **74**, 4659 (1995).
[7] Y. Kitagawa *et al.*, Phys. Rev. Lett. **68**, 48 (1992).
[8] F. Amiranoff *et al.*, Phys. Rev. Lett. **74**, 5220 (1995).
[9] F. Amiranoff *et al.*, Phys. Rev. Lett. **81**, 995 (1998).
[10] E. Takahashi *et al.*, J. Phys. Soc. Jpn. (to be published).
[11] H. Hamster *et al.*, Phys. Rev. Lett. **71**, 2725 (1993).
[12] J. R. Marques *et al.*, Phys. Rev. Lett. **76**, 3566 (1996).
[13] C. W. Siders *et al.*, Phys. Rev. Lett. **76**, 3570 (1996).
[14] E. Tokunaga, A. Terasaki, and T. Kobayashi, Opt. Lett. **17**, 1131 (1992).
[15] J. P. Geindre *et al.*, Opt. Lett. **19**, 1997 (1994).
[16] W. K. B. Panofski and W. A. Wenzel, Rev. Sci. Instrum. **27**, 976 (1956).
[17] L. M. Gorbunov and V. I. Kirsanov, Zh. Éksp. Teor. Fiz. **93**, 509 (1987) [Sov. Phys. JETP **66**, 290 (1987)].
[18] J. R. Marques *et al.*, Phys. Plasmas **5**, 1162 (1998).